A 3D finite-element model of the Adriatic tides

Benoit Cushman-Roisin*, Christopher E. Naimie

Thayer School of Engineering, Dartmouth College, Hanover, NH 03755-8000, USA

Accepted 15 August 2002

Abstract

A 3D finite-element numerical model is applied to the Adriatic Sea to simulate its tidal motions. This fully nonlinear model includes a free surface, very realistic topography, and an advanced turbulence closure. Comparison with available tidal elevations at coastal stations and with tidal ellipses at a few locations in the open sea demonstrates that the model simulations are highly accurate. The results are then used to determine the 3D distribution of the tidal residual currents.
© 2002 Published by Elsevier Science B.V.

Keywords: Finite-element model; Adriatic Sea; Tidal residual currents

1. Introduction

The Adriatic Sea is a semi-enclosed sea bordered by Italy on the west and by former Yugoslavian republics and Albania on the east, and communicating with the remainder of the Mediterranean Sea at its southern end (Fig. 1). It forms an elongated basin, approximately 800 km long and 200 km wide, which can be divided into three distinct regions generally known as the northern, middle, and southern Adriatic (Artegiani et al., 1997). The northern Adriatic lies on the continental shelf, which slopes gently southwards to a depth of 100 m. The middle Adriatic begins where the bottom drops abruptly from 100 m to over 250 m in several locations collectively known as the Pomo Depressions, also called the Jabuka Pit, and ends where the bottom rises

again to approximately 150 m at the Palagruza (Pelagosa) Sill, located at the narrowest section between Vieste (Italy) and slightly north of Dubrovnik (Croatia). Finally, the southern Adriatic, from the Palagruza Sill to the Strait of Otranto (75 km wide and 780 m deep), is characterized by an abyssal basin called the South Adriatic Pit, with maximum depth exceeding 1300 m. In contrast to the Italian coast, which describes gentle curves accompanied by a structured bottom slope, the Croatian coast is torn by channels and islands of very irregular topography.

Unlike the rest of the Mediterranean Sea, where tides are very weak, the Adriatic has moderate tides, with the highest amplitudes reaching 26.6 cm at the M2 frequency (12.421 h) and 20.1 cm at the K1 frequency (23.934 h), both in the Gulf of Trieste (northeastern corner). A summary of the tidal amplitudes and phases along both eastern and western coasts for the seven most important constituents (M2, S2, K1, O1, P1, N2, and K2) can be found in Polli (1960), supplemented by Mosetti (1987) and

* Corresponding author. Tel.: +1-603-646-3248; fax: +1-603-646-3856.
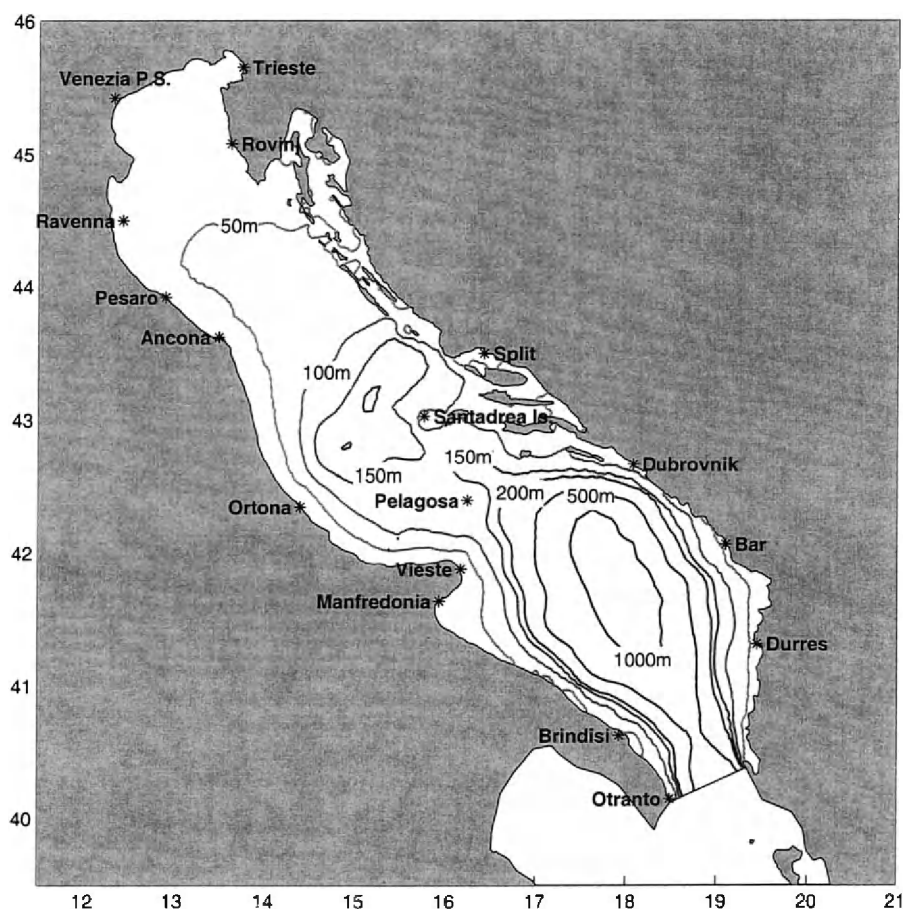*E-mail address:* benoit.r.roisin@dartmouth.edu (B. Cushman-Roisin).

Fig. 1. Geography and bathymetry of the Adriatic Sea. Stars indicate the locations of the tidal stations from which data were used for the evaluation of the model results.

Tsimplis et al. (1995). Fig. 2 shows the spatial structure of the M2 and K1 tides inferred from coastal data by Polli (1960). Table 1 recapitulates tide-gage coastal data from these various authors.

Relatively little is known about tidal currents in the Adriatic Sea. There exist a few reports for stations in the northern part of the basin. Cavallini (1985) extracted the M2 tidal-ellipse characteristics from currentmeter data that had been previously collected by Michelato (1983) at a series of stations in the northern Adriatic. Mosetti and Purga (1990) reported observations from four currentmeters in the Gulf of Trieste. More recently, Ursella and Gačić (2001) extracted tidal currents from ADCP observations collected during broad surveys along the Italian Coast

and center of the sea. Their results are compiled as maps of the M2 and K1 current tidal ellipses and phases, but these results are spurious. The amphidromic point of the M2 tide lies far to the south of where Polli (1960) found it, and the tidal ellipses differ significantly between summer and winter, which should not be the case.

Scattered data of tidal currents exist for the Croatian channels: Zore-Armanda (1979) for the Brač Channel (8 cm/s) and Viški Channel (>8 cm/s), Bone (1986) for the Vir Sea (4.8 cm/s near the surface and 2.5 cm/s near the bottom for semidiurnal tide, and 1.5 and 1.4 cm/s, respectively, for the diurnal tide), and Vilibić and Orlić (1999) for the Pasman Channel (10 cm/s near the surface for M2).
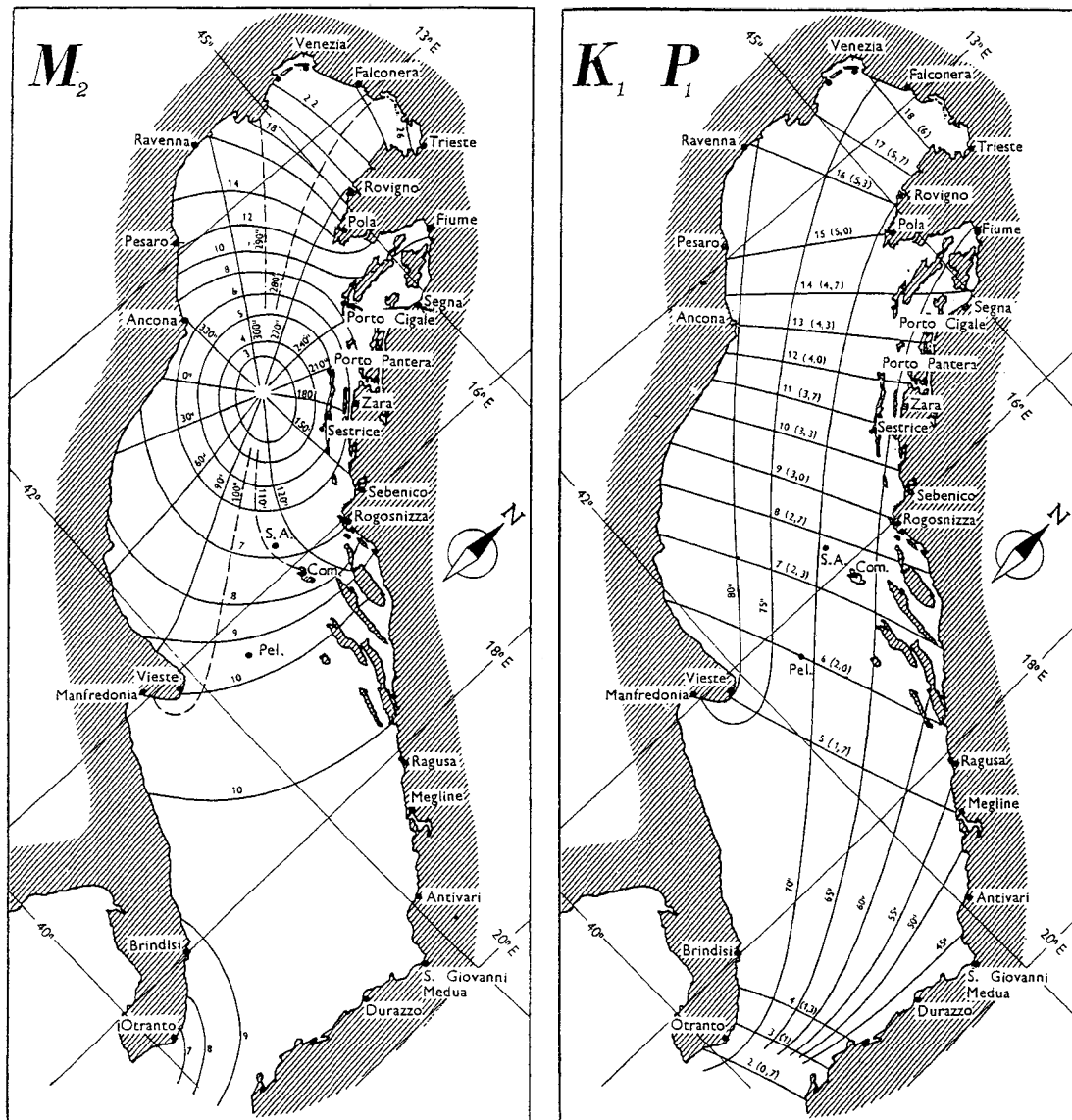
Fig. 2. Semidiurnal (M2) and diurnal (K1-P1) tidal components across the Adriatic derived from coastal observations (according to Polli, 1960).

Many calculations of the Adriatic tides have been performed over the years, starting with several calculations made by pen and paper in the pre-computer era. Most noteworthy are the works of Sterneck (1915, 1919) and Defant (1920), who defined 40 cross-sections along the axis of the basin and integrated the frictionless hydrodynamical equations suitably discretized over those intervals.

Accerboni and Manca (1973) receive credit for the first computer model of the Adriatic tides. This was a 2D storm-surge model based on a uniform finite-difference grid covering the entire sea, with 20-km resolution and no islands; the dynamics were linear, except for quadratic friction. This model was the first and, until now, also the only tidal computer model for the entire Adriatic Sea.

Table 1
Tidal-gage data for the primary constituents in the Adriatic Sea

Place	LON	LAT	M2		S2		K1		O1		P1		N2		K2	
			amp	pha	amp	pha	amp	pha	amp	pha	amp	pha	amp	pha	amp	pha
Otranto	18.50	40.15	0.065	110	0.040	116	0.025	83	0.011	58	0.008	72	0.012	104	0.017	118
Brindisi	17.93	40.63	0.087	102	0.052	111	0.046	69	0.015	57	0.015	69	0.014	99	0.014	111
Manfredonia	15.94	41.64	0.100	113	0.061	119	0.047	78	0.017	49	0.017	66	0.016	120	0.027	119
Vieste	16.18	41.88	0.079	89	0.051	113	0.042	80	0.016	84	0.015	66	0.019	76	0.019	104
Ortona	14.40	42.35	0.064	97	0.045	106	0.097	88	0.034	67	0.030	84	0.009	91	0.021	103
Ancona	13.50	43.62	0.060	345	0.032	358	0.128	93	0.040	80	0.041	95	0.013	333	0.002	355
Pesaro	12.92	43.92	0.128	311	0.068	313	0.154	84	0.051	84	0.042	56	0.032	279	0.018	313
Ravenna	12.43	44.50	0.155	303	0.091	310	0.159	82	0.050	67	0.053	82	0.030	296	0.025	310
Venezia P.S.	12.33	45.42	0.221	320	0.124	328	0.185	87	0.061	76	0.052	101	0.039	320	0.057	325
Trieste	13.75	45.65	0.259	277	0.152	285	0.197	74	0.061	56	0.052	72	0.044	280	0.063	283
Rovinj	13.63	45.08	0.178	263	0.100	270	0.175	67	0.058	50	0.047	63	0.031	263	0.045	269
Split	16.43	43.50	0.076	121	0.054	122	0.095	55	0.032	36	0.027	47	0.011	124	0.021	122
Dubrovnik	18.08	42.67	0.087	104	0.058	109	0.055	60	0.021	40	0.016	51	0.015	106	0.021	110
Bar	19.10	42.07	0.092	105	0.056	110	0.048	57	0.019	63	0.014	33	0.013	114	0.017	108
Durres	19.45	41.32	0.093	102	0.055	104	0.050	48	0.016	48	0.014	27	0.006	123	0.015	114
Santadrea Is.	15.77	43.03	0.068	93	0.044	95	0.068	54	0.025	42	×	×	×	×	×	×
Pelagosa	16.25	42.40	0.100	103	0.059	115	0.060	71	0.030	58	0.030	48	0.030	104	0.030	103

Stations are listed counterclockwise around the Adriatic Sea, followed by islands. Tidal elevations are in meters.

Adapting the model of Accerboni and Manca (1973) to the northern basin, McHugh (1974) was able to stimulate the tides with higher resolution (7.5 km). This model successfully reproduced the M2 tide at a few northern ports, although the amplitudes were overpredicted (by about 5%); for the K1 tide, the model was far less successful, presumably because of an inadequate boundary condition along the open side.

A decade passed before the next attempt when Cavallini (1985) used a 3D model. This model retained linear continuity and momentum equations, but had a quadratic law for bottom friction. The domain was again the northern basin (down to the line from Pesaro on the Italian side to Pula on the Croatian side), and the horizontal resolution was 7.5 km. In the vertical, the equations were projected onto the first five eigenfunctions of the vertical-viscosity operator. Only the M2 tide was simulated, leaving the reader to believe that simulations of the diurnal tides were not successful. Computed currents were compared with available current observations, but whereas the directions of the computed tidal ellipses were in good agreement with the observations, the magnitude of the computed velocities exceeded the observed values by more than 50% in average.

Later investigators are Canceill (1993) and Tsimplis et al. (1995), who modeled the tides over the entire Mediterranean Sea using 2D models with nonlinear advection and quadratic friction. Because of the large extent of their simulated domains, these models had very low horizontal resolution in the Adriatic (15 and 8 km, respectively). Both computed not only the M2 tide, but also the S2, K1, and O1 tides. Comparison of computed elevations against tide-gage data at various coastal stations revealed a good agreement, but no comparison of modeled and observed currents was included in these studies.

Recently, Malačič et al. (2000) used a similar nonlinear 2D model, but for the northern Adriatic (down to the Pesaro–Pula line as in the earlier studies) with very high horizontal resolution (556 m). After calibration of open-boundary conditions, their averaged difference between simulated and observed elevations, calculated as the vectorial difference of numbers with amplitudes and phases, fell below 1.3 cm for each of the seven major tidal constituents (M2, S2, K2, K1, O1, and P1). They also estimated the tidal residual currents by taking the low-frequency component of their time series.

In the light of the preceding review, it is evident that there is a need for a sea-wide 3D high-resolution

model of Adriatic tides. The range of geographical scales, from the jagged Croatian coast to the broad features of the northern bottom slope and South Adriatic Pit, favors the use of an unstructured grid with variable mesh spacing. Thus, the finite-element method stands as the choice candidate. A fully nonlinear 3D finite-element model was developed for the study of the coastal ocean, with a first set of applications devoted to the Gulf of Maine where the tides are large (Lynch et al., 1996; Naimie, 1996). This model stands as an ideal tool to meet the need for model studies of the Adriatic Sea.

The purpose of the present article is the adaptation of the finite-element model to the Adriatic Sea and its application to tides. The text is structured as follows. Section 2 recapitulates the barotropic formulation of the model, its turbulence closure, and its numerical implementation with finite elements; then, Section 3 presents the results of tidal simulations, a comparison with available observations, and the computation of the 3D residual currents; finally, Section 4 summarizes the findings.

2. The hydrodynamical model

A detailed description of the numerical model is given by Lynch et al. (1996), and only a brief summary is provided here. The core of the model is the nonlinear 3D shallow-water equations using the hydrostatic and Boussinesq approximations. The surface is free, and the Coriolis force is included. In the barotropic version, to which we restrict our attention here, the density is taken as a constant. In the momentum equations appears an eddy viscosity, the value of which is locally determined by a turbulence-closure scheme (Mellor and Yamada, 1982) as a function of the local stratification (absent here), turbulent kinetic energy, and mixing length. The last two quantities are in turn determined by two additional equations. Horizontal diffusion of momentum follows the prescription of Smagorinsky (1963).

2.1. Governing equations

In the Cartesian coordinate system with x directed eastward, y northward, and z upward, the 3D velocity vector with components (u, v, w) obeys the following continuity and momentum equations:

$$\frac{\partial u}{\partial x} + \frac{\partial v}{\partial y} + \frac{\partial w}{\partial z} = 0, \tag{1}$$

$$\frac{\mathrm{d}u}{\mathrm{d}t} - fv = -g\frac{\partial \zeta}{\partial x} + \frac{\partial}{\partial x}\left(A\frac{\partial u}{\partial x}\right) + \frac{\partial}{\partial y}\left(A\frac{\partial u}{\partial y}\right)$$
$$+ \frac{\partial}{\partial z}\left(N_\mathrm{m}\frac{\partial u}{\partial z}\right), \tag{2}$$

$$\frac{\mathrm{d}v}{\mathrm{d}t} + fu = -g\frac{\partial \zeta}{\partial y} + \frac{\partial}{\partial x}\left(A\frac{\partial v}{\partial x}\right) + \frac{\partial}{\partial y}\left(A\frac{\partial v}{\partial y}\right)$$
$$+ \frac{\partial}{\partial z}\left(N_\mathrm{m}\frac{\partial v}{\partial z}\right). \tag{3}$$

In these equations, t is time, $\mathrm{d}/\mathrm{d}t = \partial/\partial t + u\partial/\partial x + v\partial/\partial y + w\partial/\partial z$ the material time derivative, $\zeta(x, y, t)$ is the surface elevation, f the Coriolis parameter (a constant), g the gravitational acceleration (a constant), A the horizontal eddy diffusivity (defined below), and N_m the vertical eddy viscosity (also defined below).

The sea surface elevation is determined from the vertically integrated continuity equation:

$$\frac{\partial \zeta}{\partial t} = -\frac{\partial}{\partial x}\left(\int_{-h}^{\zeta} u \, \mathrm{d}z\right) - \frac{\partial}{\partial y}\left(\int_{-h}^{\zeta} v \, \mathrm{d}z\right), \tag{4}$$

where $h(x, y)$ is the water depth at rest.

2.2. Turbulence closure

The turbulence closure scheme of Mellor and Yamada (1982) provides two evolution equations, for the turbulence kinetic energy q^2 and the mixing length l. In the particular case of a constant density, these reduce to:

$$\frac{\mathrm{d}q^2}{\mathrm{d}t} = 2N_\mathrm{m}\left[\left(\frac{\partial u}{\partial z}\right)^2 + \left(\frac{\partial v}{\partial z}\right)^2\right] - \frac{2}{B_1}\frac{q^3}{l}$$
$$+ \frac{\partial}{\partial z}\left(N_\mathrm{q}\frac{\partial q^2}{\partial z}\right), \tag{5}$$

$$\frac{\mathrm{d}q^2 l}{\mathrm{d}t} = E_1 N_\mathrm{m} l \left[\left(\frac{\partial u}{\partial z} \right)^2 + \left(\frac{\partial v}{\partial z} \right)^2 \right] - \frac{W}{B_1} q^3$$
$$+ \frac{\partial}{\partial z} \left(N_\mathrm{q} \frac{\partial q^2 l}{\partial z} \right), \tag{6}$$

where N_q is the vertical eddy diffusivity of turbulent kinetic energy.

The vertical viscosity and diffusivity are parameterized in terms of q and l:

$$N_\mathrm{m} = q l s_\mathrm{m} \tag{7a}$$

$$N_\mathrm{q} = q l s_\mathrm{q}, \tag{7b}$$

where s_m and s_q are the so-called stability functions, determined according to Galperin et al. (1988). For a constant density, these reduce to constants:

$$s_\mathrm{m} = 0.39327 \tag{8a}$$

$$s_\mathrm{q} = 0.2 \tag{8b}$$

The horizontal eddy diffusivity is a function of depth-averaged velocity gradients (Smagorinsky, 1963):

$$A = 0.28 \delta^2 \sqrt{ \left(\frac{\partial \overline{u}}{\partial x} - \frac{\partial \overline{v}}{\partial y} \right)^2 + \left(\frac{\partial \overline{v}}{\partial x} + \frac{\partial \overline{u}}{\partial y} \right)^2 }, \tag{9}$$

where δ is the local mesh size and an overbar indicates a depth average. Finally, $W(z)$ is a 'wall function' and all other variables are immutable constants (see Lynch et al., 1996 for their numerical values and other details).

2.3. Boundary conditions

For tidal simulations, the surface is free of stress, while the bottom boundary condition enforces quadratic friction based on bottom velocity (with drag coefficient set at the standard value 0.005). The turbulent kinetic energy is taken proportional to the local shear stress at both surface and bottom, while the mixing length is set to zero at the surface and to a fixed value at the bottom. Finally, the vertical velocity is required to follow the free surface at the top and the topography at the bottom.

A free-slip condition is imposed along the coast. At the open boundary (Strait of Otranto), the surface elevation is imposed as a function constructed from individual tidal elevations sampled from a larger model that includes the Ionian Sea. That other model has linear dynamics and solves for the tides in the frequency domain. It is first used in an inverse mode to determine its own open-boundary conditions (across the middle of Ionian Sea) in order to meet the observed tidal elevations at the various ports along the rim of the Adriatic Sea. Once its open-boundary conditions are calibrated in that manner, the model is used in a direct mode to determine the structure of all four major tidal components everywhere, and samples are taken across Otranto Strait as boundary conditions for the nonlinear time-dependent model of the Adriatic Sea proper. No condition is imposed on the velocity along the open boundary.

2.4. Finite-element method of solution

The numerical method of solution is based on the Galerkin weak form of the governing equations, with nodal quadrature for evaluation of the inner products. To avoid numerical instability, the surface-elevation Eq. (4) is transformed into a wave equation by first differentiating it in time and then using the momentum equations to eliminate the time derivatives of the velocity components (see Lynch and Werner, 1991 for details). The computational mesh consists of horizontal triangles, with a fixed number of points distributed along the vertical at every node. The vertical distribution of these computational points is not uniform, in order to provide finer resolution near the surface and bottom, and is moreover adjusted in time to track the movements of the free surface.

Fig. 3. Top panel: Locations of depth soundings used to construct the computational mesh (7774 soundings), placed within a slightly smoothed version of the original coastline and island data. Bottom panel: The finite-element computational mesh constructed for the model. Resolution varies from 16 km over the South Adriatic Pit, where the depth is greatest, to 2 km in the coastal zones; in total, there are 9717 nodes and 17,471 triangular elements.
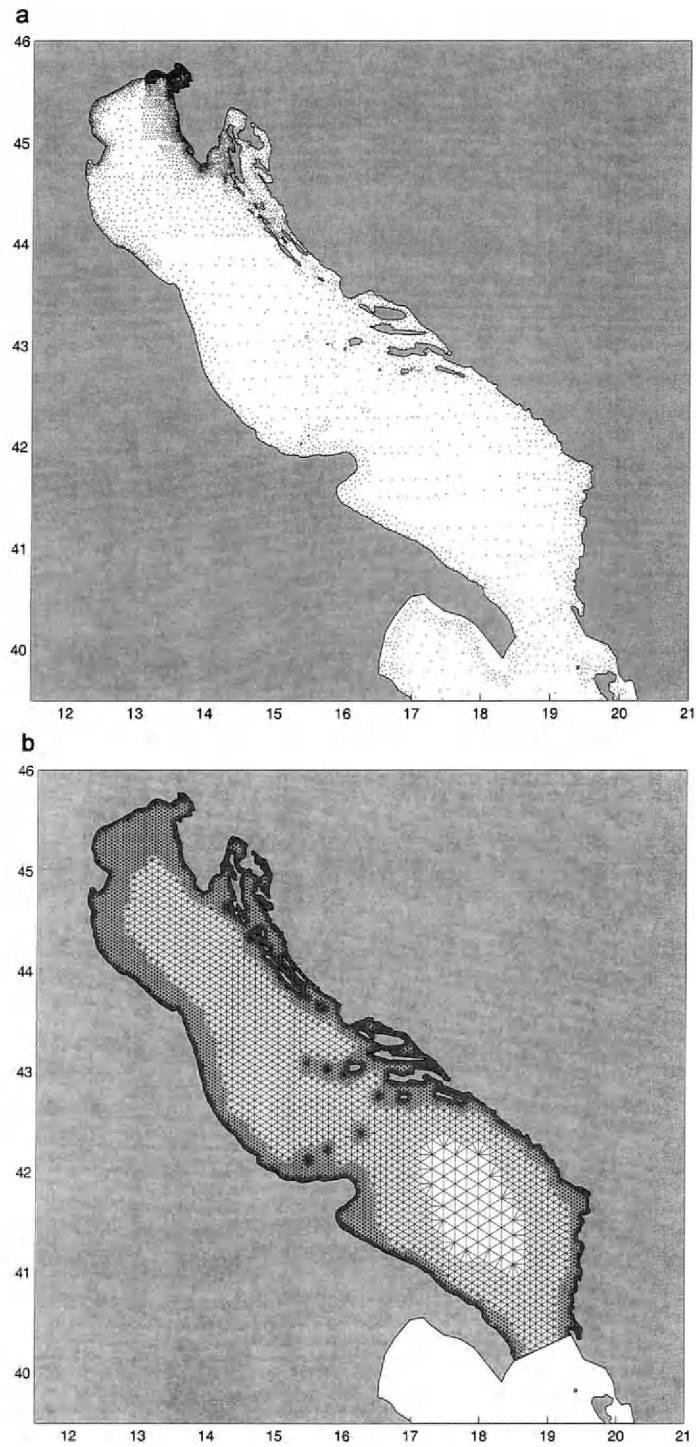
Highly detailed data of the entire Adriatic coastline and a dense array of depth soundings were compiled by and provided to us by Dr. Vlado Malačič of the Marine Biological Station in Piran, Slovenia. This data set is believed to be the most accurate one among those that are publicly available. The coastline was smoothed with a 2-km filter. Fig. 3a displays the resulting coastline, as well as the locations of the available depth soundings. The open boundary was chosen as the straight line across the Strait of Otranto that is most closely perpendicular to the isobaths. A triangular mesh was then constructed with a resolution of 16 km over the deepest part (South Adriatic Pit) and increasing gradually to 8, 4, and ultimately 2 km toward the coast. The result is a set of 17,471 triangular elements sharing 9717 nodes in the horizontal (Fig. 3b). In the vertical, we deployed 21 nodes. This high-resolution mesh is not excessive in view of the less dense set of topographic data because high resolution is required for the accurate simulation of the turbulent dissipation and the details of the currents, including the tidal residual currents.

The mesh includes a number of islands, the majority of them along the Croatian coast. In keeping with our desired resolution, islands smaller than 2 km were suppressed, and channels narrower than 2 km were closed.

3. Tidal simulations

Tidal simulations provide background currents that are predictable and exist year round. Moreover, we intend to calculate the 3D distribution of the tidal residual currents, a task which, to our knowledge, has not yet been performed for the entire Adriatic Sea.

3.1. Individual tides

Our first simulation considers only the M2 tide, which is the dominant component over the entire basin. Fig. 4 displays the result in terms of amplitude and phases (isopleths and isochrones) and can be compared to Fig. 2a. Both charts reveal the same overall features, including the presence of an amphidromic point around which the tidal wave progresses

counterclockwise. This cyclonic progression has been interpreted (Hendershott and Speranza, 1971; Cavallini, 1985; Mosetti, 1986) as a Kelvin wave travelling around the basin with the coast on its right. Rightward intensification of the currents (not shown here) further confirms this interpretation (Malačič et al., 2000).

Next, other semidiurnal and diurnal components (S2, K1, and O1) were likewise simulated, each in isolation. Together with the M2 tide, these four components form the significant tides of the Adriatic. We defer the discussion of the results and the comparison with observations to the following section, when the four major constituents are modeled simultaneously.

3.2. Superposition of major tidal components

Because tides are subject to turbulent bottom friction and because the amount of turbulence at any location depends on the near-bottom currents of all tides combined, it follows that the frictional retardation experienced by one tidal component is dependent on all other components. In other words, tidal components are coupled among one another via nonlinear friction. Nonlinear advection further links the tidal components. This coupling is particularly important for the weaker tide (S2 and O1) as they are under the influence of the larger tides (M2 and K1).

In a second series of simulations, we thus combine all four tidal components. Our simulated time is also longer (about 10 days) in order to enable an unambiguous separation of the individual tidal components from the resulting time series. Fig. 5 displays the tidal elevations and phases for the four tidal constituents, after their frequency separation. The results are qualitatively very similar to the corresponding figures of Polli (1960). Comparing with Fig. 4, we note that the structure of the M2 tide has remained virtually unchanged.

Note that both semidiurnal constituents have an amphidromic point, while both diurnal components have isopleths running across the sea and isochrones running along the main axis. As remarked earlier, the structure of the semidiurnal tide can be explained as a coastal Kelvin wave propagating counterclockwise around the basin. In contrast, the diurnal tides exhibit
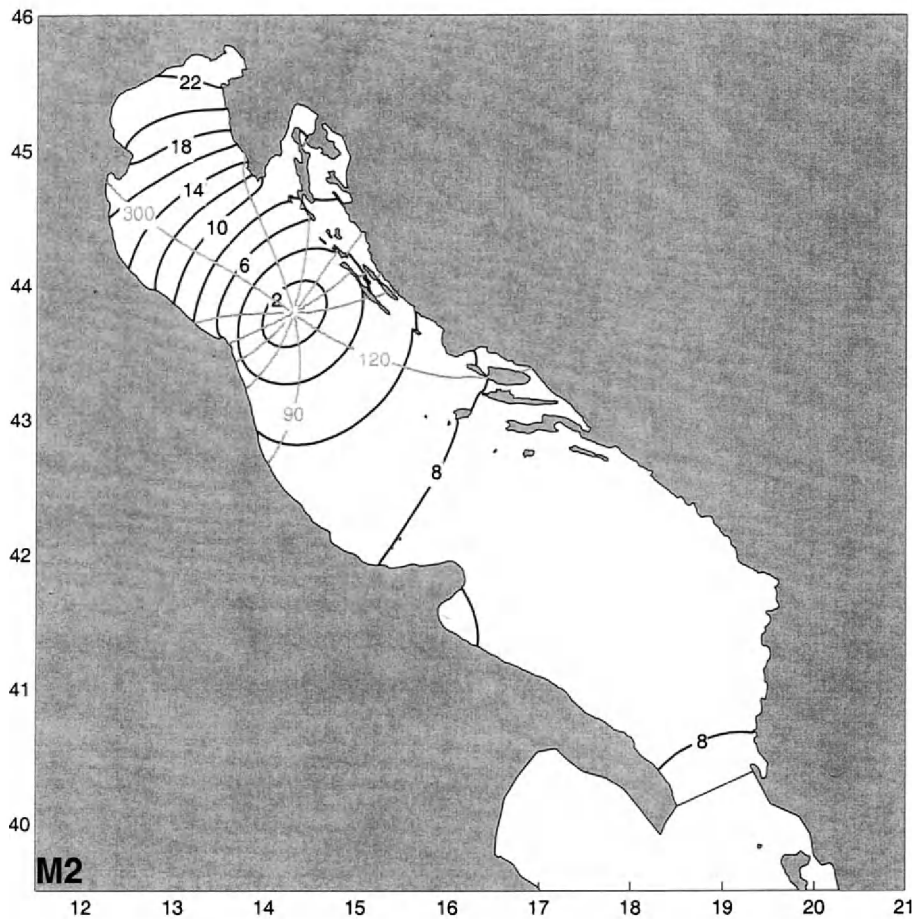
Fig. 4. Computed amplitude (solid lines, in cm) and phase (dashed lines, in degrees) of the M2 tide.

the dynamics of a topographic wave propagating across the basin from the northeast coast of Croatia to the southwest shore of Italy (Malačič et al., 2000).

Tables 2 and 3 summarize tidal elevations and their phases around the periphery of the Adriatic Sea and at a few islands, and compare the model results to the actual observations (for locations, see Fig. 1). Points of disagreement are the underestimation (by 8%) of the M2 amplitude in Trieste, and the underestimation of the K1 and O1 amplitudes (by 8% and 14%, respectively) in the northern basin (Venice to Rovinj). The inaccuracy in all phases at Venice is attributable to an observational discrepancy: data were collected at Venice proper, which lies inside a shallow lagoon behind a barrier island, while the model calculates

tidal characteristics on the offshore side of this barrier island.

Finally, the O1 phase discrepancies may appear quite large, but we have no explanation for the discrepancy aside from remarking that the O1 phases are poorly known from the observations. For example, at Trieste, Tsimplis et al. (1995) estimate the phase at 42°, while their model yields 39°, Mosetti (1987) estimates it at 56°, Godin and Trotti (1975) at 60.5°, and Polli (1960) at 62°. Slicing the long record of sea level data at Trieste from 1939 to 1992 into 648 separate sets of 29 consecutive days, Crisciani et al. (1995) estimate the O1 phase to have a mean of 61.080° and an astonishingly large standard deviation of 12.049°, the largest among all tidal components.
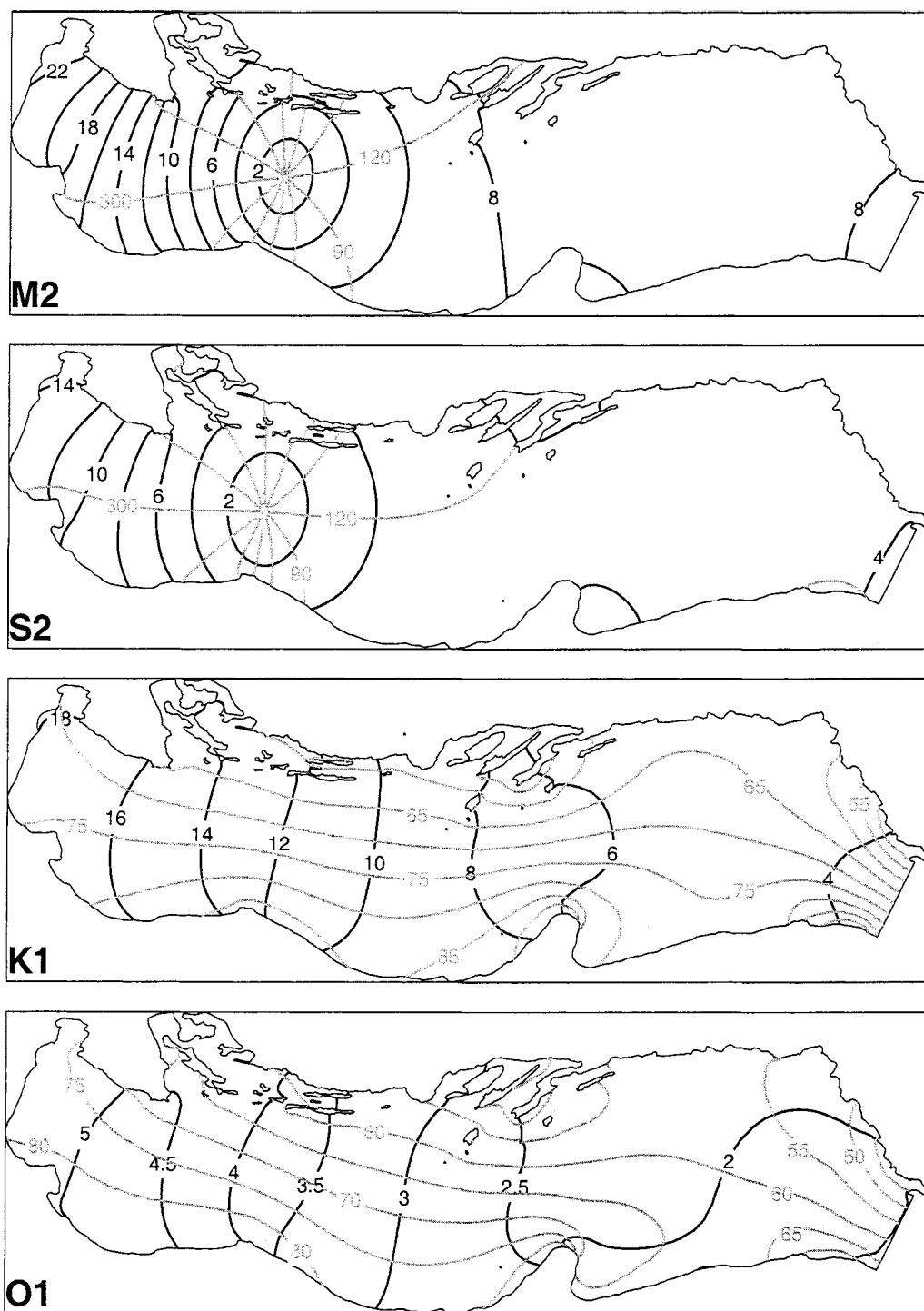
Fig. 5. Amplitude and phase distributions of the four major tidal constituents in the Adriatic Sea. Semidiurnal tides (M2 and S2) rotate counterclockwise around an amphidromic point, while the diurnal constituents (K1 and O1) progress from east to west across the basin.

Table 2
Comparison of tidal amplitudes (in cm) between model (mod) and observations (obs)

Place	M2 amplitude			S2 amplitude			K1 amplitude			O1 amplitude		
	obs	mod	diff	obs	mod	diff	obs	mod	diff	obs	mod	diff
Otranto	6.5	7.1	0.6	4.0	3.8	− 0.2	2.5	2.5	0.0	1.1	1.4	0.3
Brindisi	8.7	9.1	0.4	5.2	5.4	0.2	4.6	5.0	0.4	1.5	2.0	0.5
Manfredonia	10.0	10.4	0.4	6.1	6.4	0.3	4.7	4.5	− 0.2	1.7	1.7	0.0
Vieste	7.9	9.5	1.6	5.1	5.9	0.8	4.2	5.2	1.0	1.6	1.8	0.2
Ortona	6.4	6.9	0.5	4.5	4.9	0.4	9.7	9.4	− 0.3	3.4	3.0	− 0.4
Ancona	6.0	5.9	− 0.1	3.2	3.1	− 0.1	12.8	13.5	0.7	4.0	4.1	0.1
Pesaro	12.8	10.8	− 2.0	6.8	6.0	− 0.8	15.4	15.3	− 0.1	5.1	4.6	− 0.5
Ravenna	15.5	15.4	− 0.1	9.1	9.1	0.0	15.9	16.4	0.5	5.0	4.9	− 0.1
Venezia P.S.	22.1	21.6	− 0.5	12.4	13.2	0.8	18.5	17.8	− 0.7	6.1	5.3	− 0.8
Trieste	25.9	23.8	− 2.1	15.2	14.7	− 0.5	19.7	18.2	− 1.5	6.1	5.5	− 0.6
Rovinj	17.8	16.7	− 1.1	10.0	9.9	− 0.1	17.5	16.7	− 0.8	5.8	5.0	− 0.8
Split	7.6	8.1	0.5	5.4	5.8	0.4	9.5	9.1	− 0.4	3.2	3.0	− 0.2
Dubrovnik	8.7	9.6	0.9	5.8	5.9	0.1	5.5	5.3	− 0.2	2.1	2.1	0.0
Bar	9.2	9.6	0.4	5.6	5.8	0.2	4.8	5.2	0.4	1.9	2.1	0.2
Durres	9.3	9.4	0.1	5.5	5.6	0.1	5.0	5.2	0.2	1.6	2.1	0.5
Santadrea Is.	6.8	7.0	0.2	4.4	5.0	0.6	6.8	8.5	1.7	2.5	2.8	0.3
Pelagosa	10.0	8.7	− 1.3	5.9	5.7	− 0.2	6.0	6.9	0.9	3.0	2.4	− 0.6
mean	11.2	11.2	− 0.1	6.7	6.8	0.1	9.6	9.7	0.1	3.3	3.2	− 0.1
rms	12.6	12.2	1.0	7.4	7.5	0.4	11.1	11.0	0.8	3.7	3.5	0.4

For this comparison, all four constituents were modeled simultaneously, and the individual components were extracted from the results using a frequency-decomposition technique.

Table 3
Comparison of tidal phases (in degrees) between model (mod) and observations (obs)

Place	M2 phase			S2 phase			K1 phase			O1 phase		
	obs	mod	diff	obs	mod	diff	obs	mod	diff	obs	mod	diff
Otranto	110	112	2	116	119	3	83	85	2	58	66	8
Brindisi	102	111	9	111	119	8	69	82	13	57	67	10
Manfredonia	113	107	− 6	119	115	− 4	78	81	3	49	64	15
Vieste	89	105	16	113	115	2	80	95	15	84	79	− 5
Ortona	97	96	− 1	106	108	2	88	85	− 3	67	78	11
Ancona	345	345	0	358	362	4	93	86	− 7	80	85	5
Pesaro	311	318	7	313	327	14	84	83	− 1	84	85	1
Ravenna	303	303	0	310	310	0	82	79	− 3	67	83	16
Venezia P.S.	320	291	− 29	328	298	− 30	87	74	− 13	76	80	4
Trieste	277	281	4	285	288	3	74	69	− 5	56	75	19
Rovinj	263	274	11	270	279	9	67	66	− 1	50	70	20
Split	121	123	2	122	127	5	55	57	2	36	53	17
Dubrovnik	104	108	4	109	115	6	60	64	4	40	56	16
Bar	105	107	2	110	113	3	57	63	6	63	55	− 8
Durres	102	104	2	104	110	6	48	57	9	48	50	2
Santadrea Is.	93	114	21	95	121	26	54	67	13	42	61	19
Pelagosa	103	108	5	115	116	1	71	74	3	58	65	7
mean	174	177	3	181	185	4	72	75	2	60	69	9
rms	199	200	11	206	208	11	74	75	7	61	70	13

a

M2
     5 cm sec^{-1}

K1
     5 cm sec^{-1}
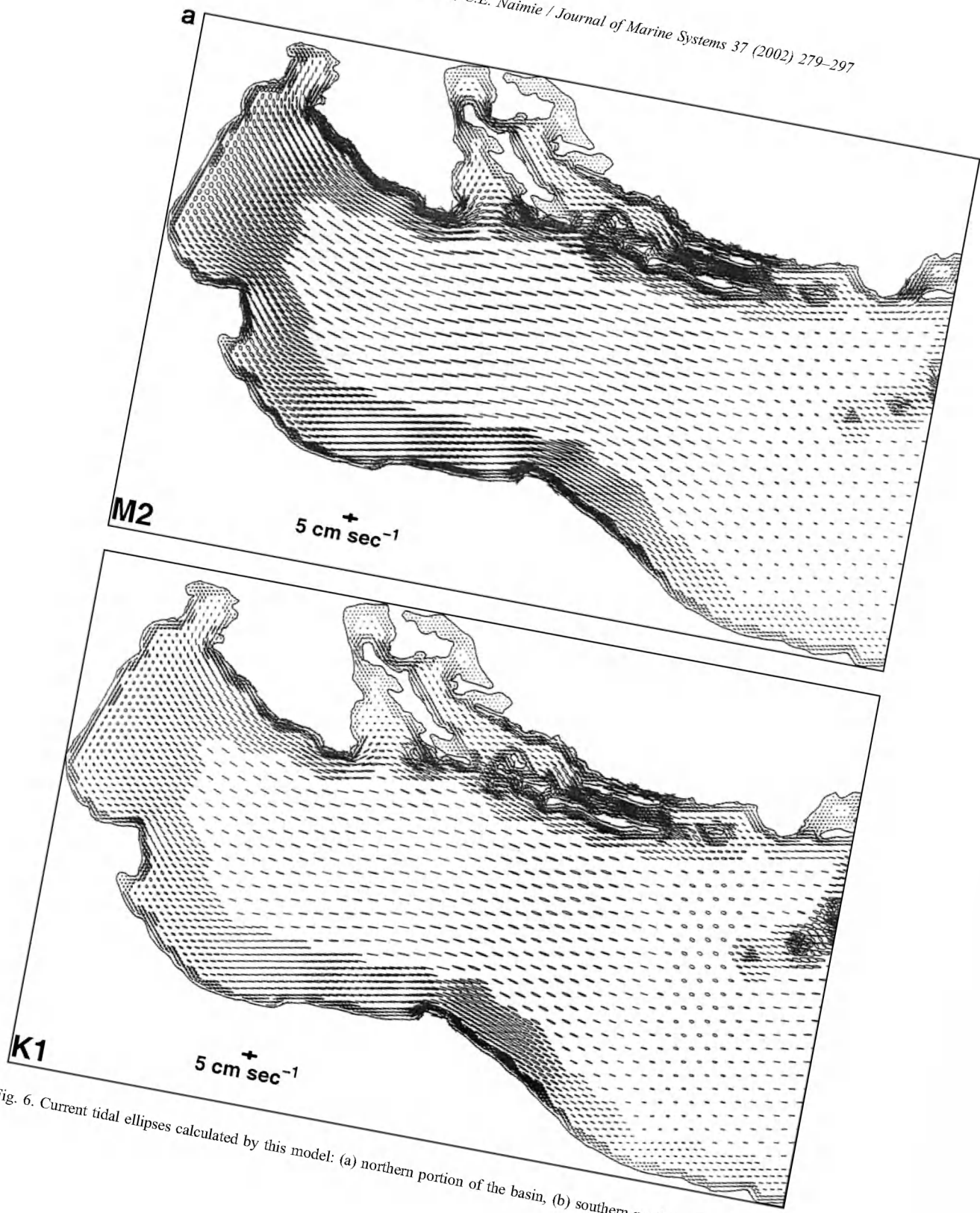
Fig. 6. Current tidal ellipses calculated by this model: (a) northern portion of the basin, (b) southern portion of the basin.
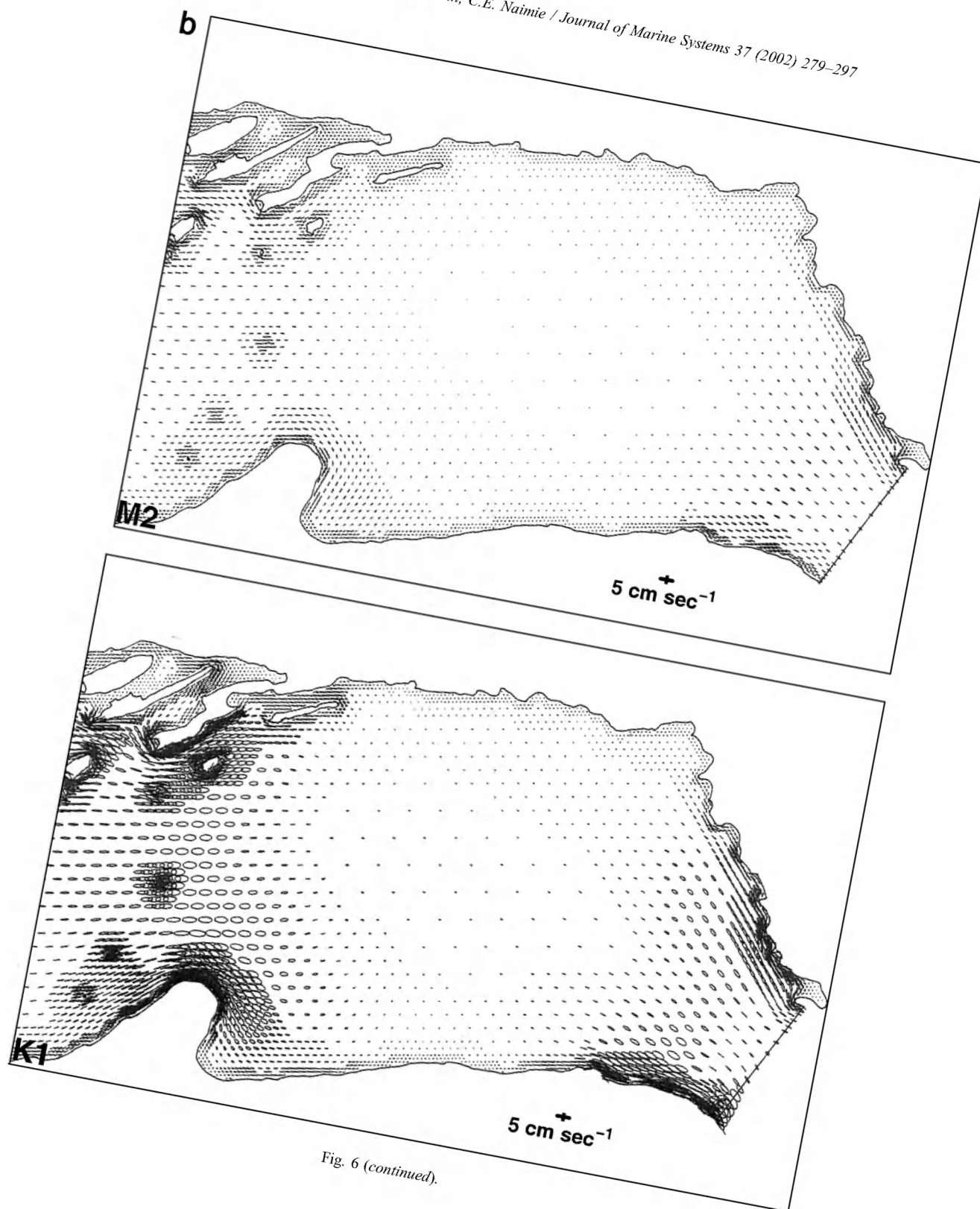
b

M2

5 cm sec⁻¹
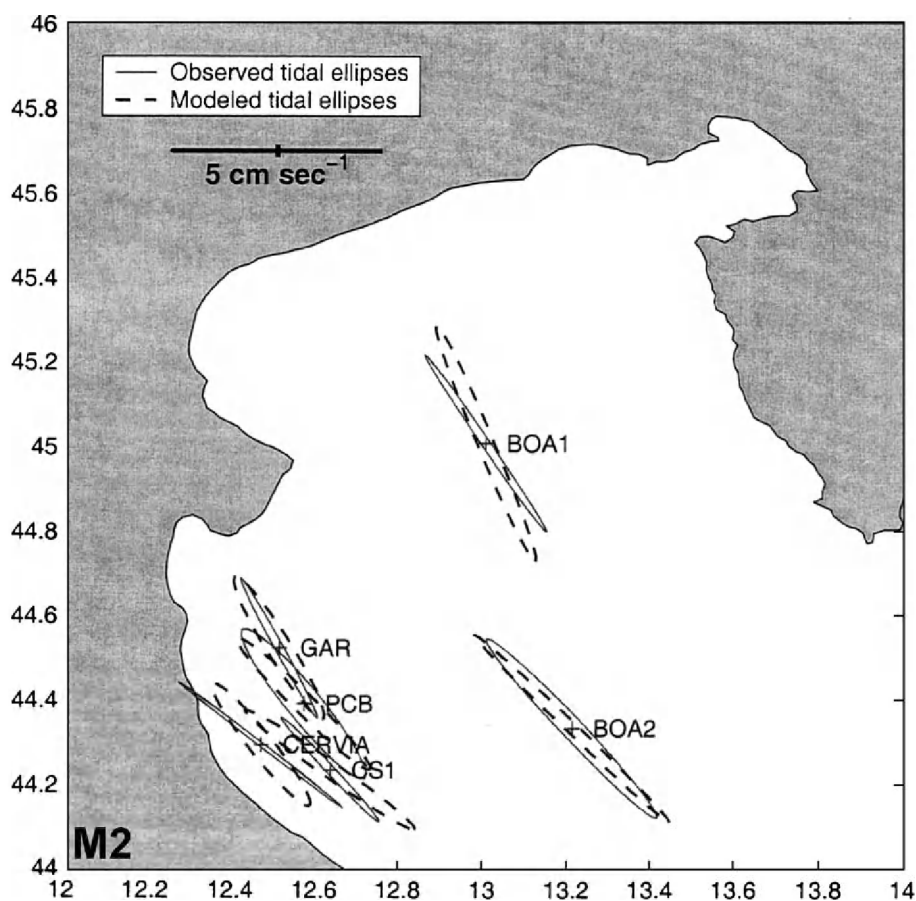
K1

5 cm sec⁻¹

Fig. 6 (continued).

Fig. 7. Comparison of M2 tidal current ellipses in the northern Adriatic. The observations were taken from Cavallini (1985), while the model results are depth-averaged.

This particular tide appears therefore to be very sensitive to something, the nature of which is unknown.

By highlighting the amplitude and phase discrepancies separately, we chose to expose more clearly the inaccuracies of our model simulations. Had we chosen

Table 4
Comparison of depth-averaged M2 tidal current ellipse parameters in the northern Adriatic with observational data from Cavallini (1985)

Place	M2 obs			M2 mod			Error (obs − mod)		
	Umaj	Umin	Ori	Umaj	Umin	Ori	Umaj	Umin	Ori
BOA1	5.1	0.2	− 55	6.1	0.4	− 67	− 1.0	− 0.2	12
BOA2	5.9	0.5	− 46	6.4	0.3	− 43	− 0.5	0.2	− 3
CERVIA	4.9	− 0.1	− 37	3.7	0.6	− 51	1.2	− 0.5	14
CS1	3.4	0.2	− 46	5.0	0.4	− 34	− 1.6	− 0.2	− 12
GAR	3.8	0.2	− 61	4.0	0.6	− 58	− 0.2	− 0.4	− 3
PCB	4.6	0.8	− 50	4.5	0.5	− 44	0.1	0.3	− 6
mean	4.6	0.3	− 49	4.9	0.4	− 49	− 0.3	− 0.1	0
rms	4.7	0.4	50	5.0	0.5	51	0.9	0.3	9

to present the errors in terms of vectorial differences, all discrepancies would have appeared significantly smaller, at the risk of masking some of the imperfections of the model simulations.

3.3. Tidal-current comparison

Tidal currents are presented in the form of tidal ellipses for both M2 and K1 tides (Fig. 6a and b—to show more details, we have placed the northern and southern basins on separate figures). Comparing these ellipses with those derived from ADCP current

data by Ursella and Gačić (2001) reveals qualitative agreement at both M2 and K1 frequencies in the northern third of the basin but significant differences elsewhere. Instead of doubting our own results, we think that the problems lie with the results of Ursella and Gačić (2001). Indeed, they find the amphidromic point of the M2 tide to be at the level of the Monte Gargano Peninsula (about 42°), which is more than a degree and a half of latitude south of where it lies according to Polli (1960), Hendershott and Speranza (1971), Mosetti (1987), Tsimplis et al. (1995), Canceill (1993), and our own simulations here (see Fig.
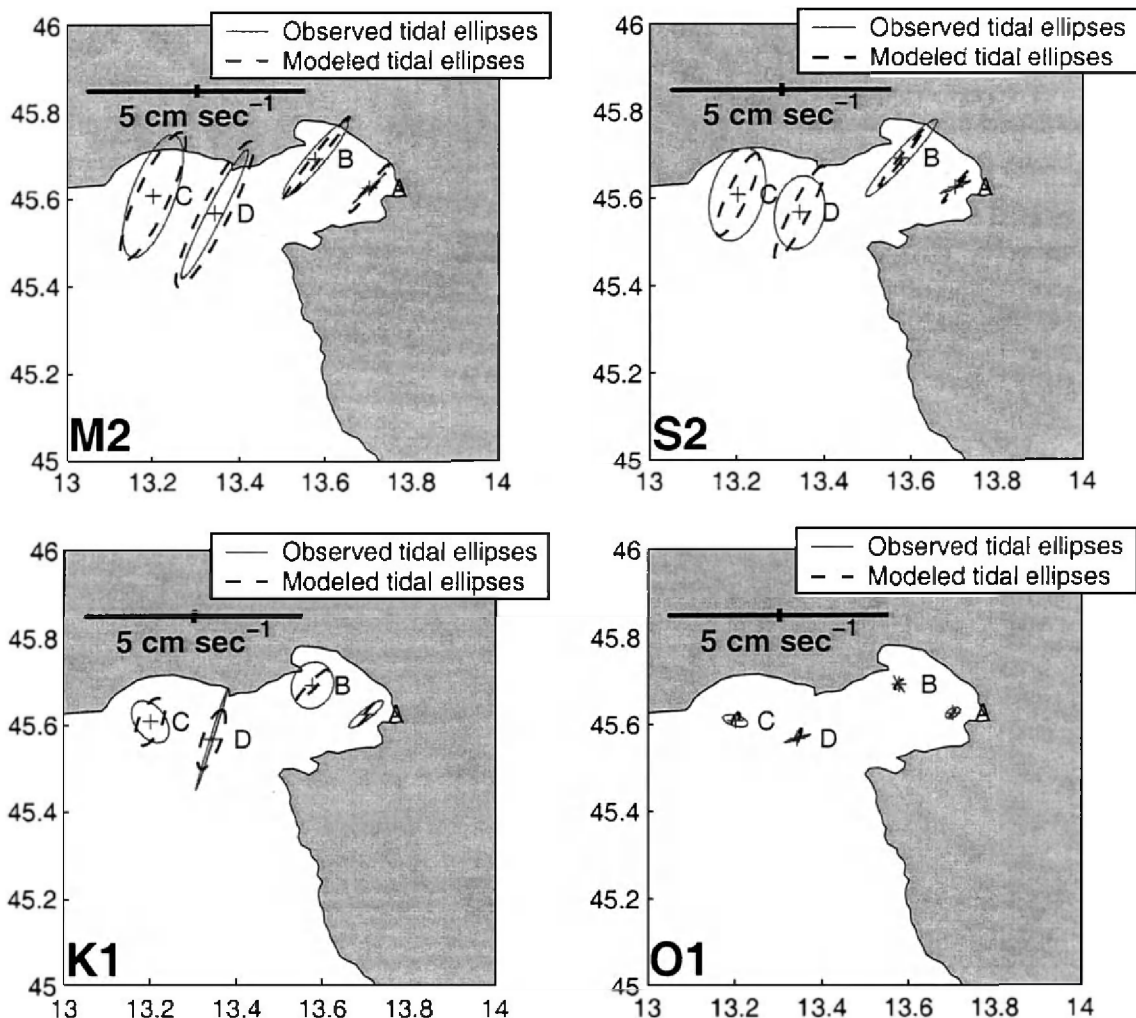

Fig. 8. Comparison of tidal currents in the Gulf of Trieste. The observations were taken from Mosetti and Purga (1990).

4). Moreover, the calculations of Ursella and Gačić (2001) lead to significant differences between summer and winter seasons, which ought not to be the case with tides. We thus suspect that they may have not properly extracted the tidal currents from their data.

However, other quantitative comparisons of tidal currents are possible. Fig. 7 and Table 4 compare observed and modeled M2 tidal current ellipses for the six stations investigated by Cavallini (1985). For the purpose of comparison, the Cavallini data are averaged over the several depths for which measure-

ments were reported, while the model results are vertically averaged. As the figure and table reveal, the agreement is good in both amplitudes and directions, except at stations CERVIA and BOA1. At these shallower locations (22 and 35 m, respectively), the model predicts currents with very similar levels of kinetic energies $[(u^2 + v^2)/2]$, but with significantly more rotation than in the actual currents. The reason for the discrepancy is not clear, and we only surmise that the model misses localized channeling of tidal currents where narrow topographic asperities are unresolved by its grid. However, it might also be that in the

Table 5

Comparison of depth-averaged M2 tidal current ellipse parameters in the Gulf of Trieste with observational data from Mosetti and Purga (1990)

Place	M2 obs			M2 mod			Diff (obs − mod)		
	Umaj	Umin	Ori	Umaj	Umin	Ori	Umaj	Umin	Ori
A	1.04	0.01	43	1.45	0.12	51	− 0.41	− 0.11	− 8
B	2.31	0.40	49	2.53	0.17	51	− 0.22	0.23	− 2
C	3.00	1.02	70	3.23	0.74	65	− 0.24	0.28	5
D	3.32	0.36	63	3.75	0.64	63	− 0.43	− 0.29	0
mean	2.42	0.45	56	2.74	0.42	58	− 0.32	0.03	− 1
rms	2.57	0.58	57	2.87	0.50	58	0.34	0.24	5

Place	S2 obs			S2 mod			Diff (obs − mod)		
	Umaj	Umin	Ori	Umaj	Umin	Ori	Umaj	Umin	Ori
A	0.77	0.06	23	0.94	0.07	51	− 0.17	− 0.01	− 28
B	2.42	0.33	47	1.67	0.09	52	0.75	0.25	− 5
C	2.20	1.23	76	2.11	0.47	65	0.09	0.76	10
D	1.72	1.12	79	2.43	0.40	63	− 0.71	0.73	16
mean	1.78	0.69	56	1.79	0.26	58	− 0.01	0.43	− 2
rms	1.89	0.85	61	1.87	0.31	58	0.53	0.54	17

Place	K1 obs			K1 mod			Diff (obs − mod)		
	Umaj	Umin	Ori	Umaj	Umin	Ori	Umaj	Umin	Ori
A	0.99	0.23	38	0.69	0.07	53	0.30	0.16	− 15
B	1.11	0.97	63	1.05	0.17	45	0.05	0.80	18
C	1.11	0.70	− 52	1.18	0.55	66	− 0.07	0.15	− 119
D	2.45	− 0.07	73	1.46	0.43	70	0.98	− 0.50	3
mean	1.41	0.46	30	1.10	0.31	58	0.32	0.15	− 28
rms	1.54	0.61	58	1.13	0.36	59	0.52	0.48	60

Place	O1 obs			O1 mod			Diff (obs − mod)		
	Umaj	Umin	Ori	Umaj	Umin	Ori	Umaj	Umin	Ori
A	0.38	− 0.21	33	0.22	0.02	50	0.16	− 0.22	− 18
B	0.45	− 0.01	− 57	0.29	0.08	45	0.16	− 0.09	− 102
C	0.59	− 0.25	− 16	0.41	0.12	68	0.18	− 0.37	− 84
D	0.63	− 0.05	17	0.51	0.09	65	0.12	− 0.14	− 48
mean	0.51	− 0.13	− 6	0.36	0.08	57	0.16	− 0.21	− 63
rms	0.52	0.16	35	0.37	0.09	58	0.16	0.23	71

presence of strong vertical shear, the observational samples (at only two levels in the vertical) are not sufficiently representative of the depth-averaged currents.

Fig. 8 and Table 5 show a similar comparison with the data reported by Mosetti and Purga (1990) for the Gulf of Trieste. Here, data for the four most significant tidal frequencies are available. The agreement is excellent at the leading (M2) frequency and almost as good at the other semidiurnal (S2) frequency. For the K1 frequency, the agreement is good at two of the four stations. At Station B, the modeled ellipse is too eccentric, while the observations at Station D indicate a highly unidirectional current that stands in contrast to the rotating currents reported at the same frequency

in close vicinity and at the same location for other frequencies. We suspect that the observations at Station D are unreliable for the K1 frequency. Finally, for the O1 frequency, observations and simulations show very comparable levels of activity, but the phases and eccentricities are not correctly captured by the model. In other words, the weak O1 tide marks the limit of the numerical model.

3.4. Tidal residuals

From the nonlinear simulations of the combined tides, one can extract the zero-frequency response, which corresponds to the tidal residuals (Lynch and Naimie, 1993). Fig. 9 presents the depth-averaged
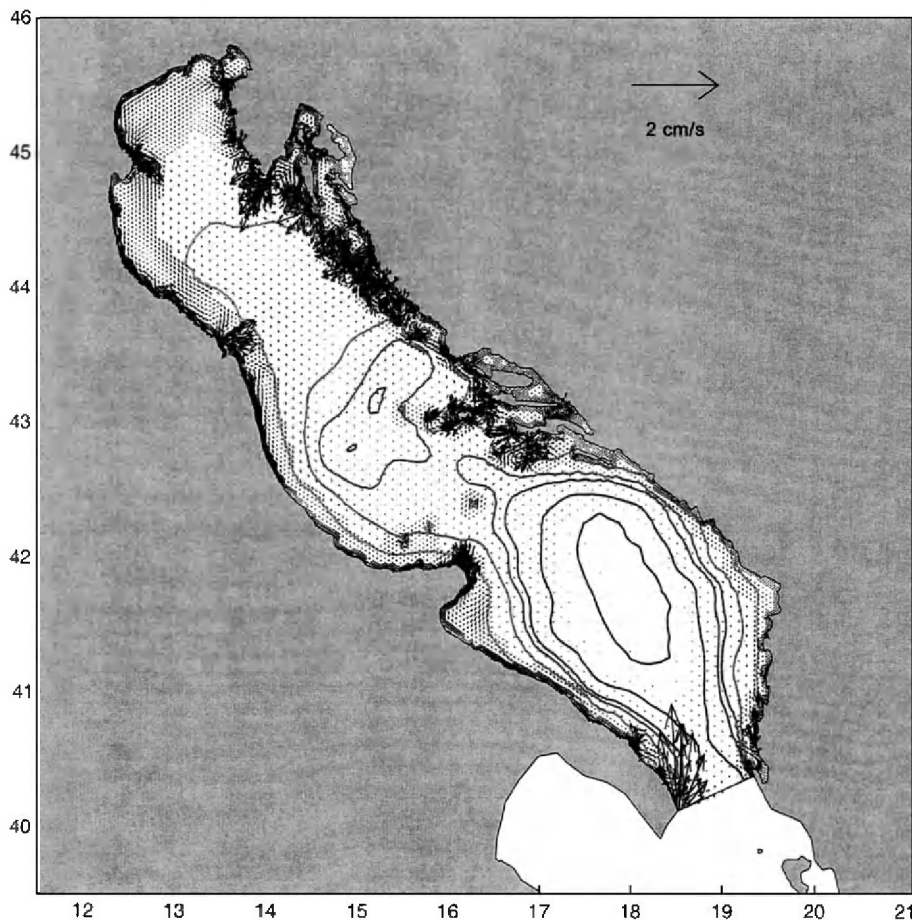

Fig. 9. Depth-averaged residual currents. Note that the largest velocities occur in the vicinity of high-curvature points along the coastline.

residual currents. Overall, these currents are far weaker than the ebb and flood currents of the M2 and K1 tides, being on the order of only a fraction of a centimeter per second. Tidal residuals are nonetheless significant in the vicinity of sharp corners of the coast, especially near the Po River delta, along the broken coast of Croatia, and around its islands. In those locations, residual currents can reach up to 1 cm/s and may be the significant motions in times of weak wind-driven and river-plume flow. Malačič et al. (2000) estimated residual tidal currents in the northern Adriatic Sea but provided only speeds, not directions. They, too, obtained low values everywhere except in rugged shallow areas. Just offshore of the Venice–Trieste coastline, they obtained values reaching 3 cm/s at isolated spots, where their higher resolution model presumably incorporated localized topographic details not retained in our sea-wide model.

Because tidal residual currents are unidirectional and persistent, they may contribute in a non-negligible way to the transport of pollutants. As for other coastal areas, however, details of the tidal residual currents depend on the bottom topography, on the degree of advective nonlinearity, and also on the level of dissipation. This third factor depends on the level of turbulence actually occurring in the water column and is thus dependent on what else is simultaneously taking place in the sea, such as wind stirring, river-plume mixing, winter convection, etc. There exists therefore an irreducible level of uncertainty.

4. Conclusions

In this article, we adapted a 3D, finite-element, free-surface numerical model to the whole Adriatic Sea. The horizontal resolution varies from 16 km over the South Adriatic Pit (where the depth exceeds 1300 m) to 2 km along the coast and in the vicinity of islands. At every horizontal node, the model also has 21 levels in the vertical. The high-resolution mesh is not excessive in view of the less dense set of topographic data because the higher the model resolution, the better modeled are the turbulent dissipation and the details of the currents, including the tidal residual currents.

In this application, the model was used in the barotropic mode (uniform density but vertically sheared currents), and the four major tidal components (M2, S2, K1, and O1) were simulated, first individually and the simultaneously. Comparisons with available observations reveal that the model is performing well. The tidal simulations presented here are believed to be the most accurate to date for the entire Adriatic Sea. They are also the only ones known to have been obtained from a 3D model covering the entire sea.

Finally, the 3D residual currents were calculated. These currents are relatively weak, except around sharp capes, which abound along the Croatian coast. This marks the first time that tidal residual currents have been calculated for the Adriatic outside of its northern basin.

The success of the present tidal simulations indicates that the finite-element model is performing adequately in the barotropic mode. The advantage of its unstructured grid (as opposed to a finite-difference model, even one with a curvilinear grid) is the potential for higher resolution in areas of complex bathymetry. It is because of this specific advantage that the model could reveal the existence of strong tidal residual currents in the vicinity of sharp angles of the coastline.

Finally, the successful simulations reported here, which are driven by no forcing other than tidal elevations imposed at the sea entrance, permit the rejection of the hypothesis first made by Sterneck (1919) and reiterated four decades later by Mosetti (1959) that the astronomical forcing (gravitational pull by moon and sun) within the Adriatic proper is an important contributor to its tidal motions. The further suggestion of Filloux (1974) that the Adriatic Sea exports tidal energy through the Strait of Otranto because the local forcing exceeds the loss to friction inside the sea can, too, be rejected with some confidence.

Acknowledgements

References

Accerboni, E., Manca, B., 1973. Storm surges forecasting in the Adriatic Sea by means of a two-dimensional hydrodynamical model numerical model. Boll. Geofis. Teor. Appl. 15, 3–22.

Artegiani, A., Bregant, D., Paschini, E., Pinardi, N., Raicich, F., Russo, A., 1997. The Adriatic Sea general circulation. Part I: Air–sea interactions and water mass structure. J. Phys. Oceanogr. 27, 1492–1514.

Bone, M., 1986. On the profile of tidal currents in the northern Adriatic. Acta Adriat. 27, 5–14.

Canceill, P., 1993. Restitution subdécymétrique des marées dans l'Océan Pacifique par un modèle hydrodynamique aux éléments finis. Thesè de Doctorat, Université Paul Sabatier, Toulouse (France) 327 pp.

Cavallini, F., 1985. A three-dimensional numerical model of tidal circulation in the northern Adriatic Sea. Boll. Oceanol. Teor. Appl. 3, 205–218.

Crisciani, F., Ferraro, S., Patti, B., 1995. Do tidal harmonic constants depend on mean sea level? An investigation for the Gulf of Trieste. Nuovo Cim. 18C, 15–18.

Defant, A., 1920. Ann. Hydrogr. Marit. Meteorol. 48, 163–169 (Berlin).

Filloux, J.H., 1974. Gravitational driving and energy of Adriatic tides. Nature 252, 566–568.

Galperin, B., Kantha, L.H., Hassid, S., Rosati, A., 1988. A quasi-equilibrium turbulent energy model for geophysical flows. J. Atmos. Sci. 45, 55–62.

Godin, G., Trotti, L., 1975. Trieste water levels 1952–1971. A study of the tide, mean level and seiche activity. Misc. Spec. Pub. 28. Department of the Environment, Fisheries and Marine Service, Ottawa, Ontario. 24 pp.

Hendershott, M.C., Speranza, A., 1971. Co-oscillating tides in long, narrow bays; the Taylor problem revisited. Deep-Sea Res. 18, 959–980.

Lynch, D.R., Werner, F.E., 1991. Three-dimensional hydrodynamics on finite elements. Part II: non-linear time-stepping model. Int. J. Numer. Methods Fluids 12, 507–533.

Lynch, D.R., Naimie, C.E., 1993. The M2 tide and its residual on the outer banks of the Gulf of Maine. J. Phys. Oceanogr. 23, 2222–2253.

Lynch, D.R., Ip, J.T.C., Naimie, C.E., Werner, F.E., 1996. Comprehensive coastal circulation model with application to the Gulf of Maine. Cont. Shelf Res. 16, 875–906.

Malačič, V., Viezzoli, D., Cushman-Roisin, B., 2000. Tidal dynamics in the northern Adriatic Sea. J. Geophys. Res. 105, 26265–26280.

McHugh, G.F., 1974. A numerical model for two tidal components in the northern Adriatic Sea. Boll. Geofis. Teor. Appl. 16, 322–331.

Mellor, G.L., Yamada, T., 1982. Development of a turbulence closure model for geophysical fluid problems. Rev. Geophys. Space Phys. 20, 851–875.

Michelato, A., 1983. Caratteristiche della circolazione delle acque costiere dell'Emilia-Romagna. Atti del Convegno "Eutrofizzazione dell' Adriatico-Ricerche e linee di intervento", Bologna, 18–20 May 1983, 149–168.

Mosetti, F., 1959. Sul calcolo dei filtri per l'analisi periodale col metodo delle combinazioni lineari di ordinate. Boll. Oceanol. Teor. Appl. 1, 235–308.

Mosetti, F., 1987. Distribuzione delle maree nei mari italiani. Boll. Oceanol. Teor. Appl. 5, 65–72.

Mosetti, F., Purga, N., 1990. Courants côtiers de différente origine dans un petit golfe (Golfe de Trieste). Boll. Oceanol. Teor. Appl. 8, 51–62.

Mosetti, R., 1986. Determination of the current structure of the M2 tidal component in the northern Adriatic by applying the rotary analysis to the Taylor problem. Boll. Oceanol. Teor. Appl. 4, 165–172.

Naimie, C.E., 1996. Georges Bank residual circulation during weak and strong stratification periods: prognostic numerical model results. J. Geophys. Res. 101, 6469–6486.

Polli, S., 1960. La Propagazione delle Maree nell'Adriatico. Atti del Convegno dell' Associazione Geofisica Italiana, Roma 1959. 11 pp.

Smagorinsky, J., 1963. General circulation experiments with the primitive equations I. The basic experiment. Mon. Weather Rev. 91, 99–164.

Sterneck, R., 1915. Zur hydrodynamischen Theorie der Adriagezeiten. Sitzungsber. Kais. Akad. Wiss. Wien 124, 147–180.

Sterneck, R., 1919. Die Gezeitenerscheinungen der Adria—II. Teil. Die theoretische Erklärung der Beobachtungstatsachen. Denkschr. Akad. Wiss. Wien 96, 277–324.

Tsimplis, M.N., Proctor, R., Flather, R.A., 1995. A two-dimensional tidal model for the Mediterranean Sea. J. Geophys. Res. 100, 16223–16239.

Ursella, L., Gačić, M., 2001. Use of the acoustic Doppler current profiler (ADCP) in the study of the circulation of the Adriatic Sea. Ann. Geophys. 19, 1183–1193.

Vilibić, I., Orlić, M., 1999. Surface seiches and internal Kelvin waves observed off Zadar (East Adriatic). Estuar. Coast. Shelf Sci. 48, 125–136.

Zore-Armanda, M., 1979. Fizičke karakteristike mora u području otoka Hvara (Physical characteristics of the sea-water in the region of the Island of Hvar). Acta Biol. 8, 65–78.